

Refine and Represent: Region-to-Object Representation Learning

Akash Gokul^{1*}, Konstantinos Kallidromitis^{2*}, Shufan Li^{1*},
Yusuke Kato³, Kazuki Kozuka³, Trevor Darrell¹, and Colorado J Reed¹

¹Berkeley AI Research

²AI Lab, Panasonic R&D Company of America

³Digital and AI Technology Center, Technology Division, Panasonic Holdings Co.
{akashgokul, jacklishufan}@berkeley.edu, k.kallidromitis@us.panasonic.com

Abstract

Recent works in self-supervised learning have demonstrated strong performance on scene-level dense prediction tasks by pretraining with object-centric or region-based correspondence objectives. In this paper, we present Region-to-Object Representation Learning (*R2O*) which unifies region-based and object-centric pretraining. *R2O* operates by training an encoder to dynamically refine region-based segments into object-centric masks and then jointly learns representations of the contents within the mask. *R2O* uses a *region refinement module* to group small image regions, generated using a region-level prior, into larger regions which tend to correspond to objects by clustering region-level features. As pretraining progresses, *R2O* follows a *region-to-object curriculum* which encourages learning region-level features early on and gradually progresses to train object-centric representations. Representations learned using *R2O* lead to state-of-the-art performance in semantic segmentation for PASCAL VOC (+0.7 mIOU) and Cityscapes (+0.4 mIOU) and instance segmentation on MS COCO (+0.3 AP^{mk}). Further, after pretraining on ImageNet, *R2O* pretrained models are able to surpass existing state-of-the-art in unsupervised object segmentation on the Caltech-UCSD Birds 200-2011 dataset (+2.9 mIOU) without any further training. We provide the code/models from this work at <https://github.com/KKallidromitis/r2o>.

1 Introduction

Recent progress in self-supervised pretraining in computer vision has led to a wide range of improvements on transfer learning tasks such as image classification, object detection, and segmentation [8, 6, 46, 28]. Instance discrimination pretext objectives have driven many of these advancements, whereby contrasting augmented views of an input image, a network learns representations that are invariant to predefined image-level data augmentations. However, much of this work has focused on scene-level pretraining, which as recent works have shown, is not optimal for many pixel-level prediction tasks, such as semantic segmentation [56, 63, 28].

Many state-of-the-art methods have extended image-level pretraining to learn local features by leveraging either region-based [56, 60] or object-centric similarity tasks [28, 2]. Region-based pretraining methods enforce predictive invariance between random image patches that are present in both views and thus learn from all regions in an image, regardless of size or content. Similarly, object-centric pretraining uses segmentation heuristics to localize objects and enforces representational invariance to the features corresponding to the objects in the scene. Both types of representation learning have led to improvements in downstream dense prediction tasks [28, 2, 57, 65].

*Denotes co-first authorship where co-first authors can prioritize their names when referencing this paper.

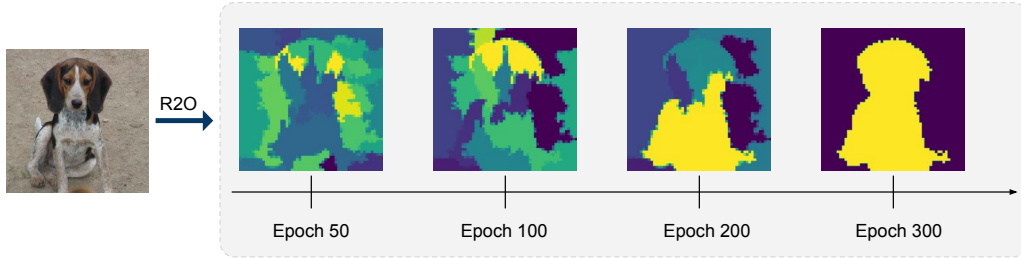


Figure 1: ***R2O* unifies region-based and object-centric pretraining by jointly learning to discover and represent regions and objects.** Our region refinement process allows object discovery using scheduled K-means clustering over the embeddings of neighboring regions. Following this schedule, masks early in training consist of random image segments ($K = 128$) which gradually develop into object centered masks ($K = 4$). By the end of pretraining, *R2O* enables object-centric discovery and representation without requiring advanced segmentation algorithms to localize objects in a scene.

In this paper, we find that pretraining for dense prediction tasks benefits from both region-based and object-centric objectives at different stages of the pretraining process. Specifically, we present Region-to-Object representation learning (*R2O*): a framework that learns region-based and object-centric features by dynamically refining segmentation masks throughout pretraining and identifying dense representations in these segmented regions. *R2O* uses a *region refinement module* to transform the predicted masks from multiple small scale image regions that capture consistency in color and spatial position, to larger, object-centric regions. Predicted masks are then used to enforce representational invariance for the features corresponding to the discovered segments.

Finally, we introduce a region-to-object curriculum, which gradually reduces the number of segments within predicted masks, in order to encourage region-level pretraining for small image regions early on and increasingly object-centric representation learning as pretraining progresses (see Figure 1).

We study *R2O* on a range of datasets and tasks, including object detection, instance segmentation, and semantic segmentation. Our contributions are summarized as follows:

- We present *R2O*, which unifies region-based and object-centric instance discrimination pretraining by training an encoder to dynamically refine region-based segments into object-centric masks and then jointly learns representations of the contents within the mask.
- We introduce a region-to-object pretraining curriculum for *R2O* that begins by training local features corresponding to simple image regions, e.g. adjacent pixels sharing similar color values, and gradually progresses to learn object centric features.
- *R2O* pretraining improves transfer performance in tasks such as object detection and instance segmentation on MS COCO (+0.3 AP^{mk}) as well as exceeding previous methods in PASCAL VOC (+0.7 mIOU) and Cityscapes (+0.4 mIOU) semantic segmentation. *R2O* further improves state-of-the-art unsupervised segmentation performance on Caltech-UCSD Birds 200-2011 (CUB-200-2011) by +2.9 mIoU *despite not finetuning on CUB-200-2011*.

2 Related Works

Image-level Self-Supervised Pretraining Self-supervised learning algorithms aim to learn representations from unlabelled data that are effective for a desired task, such as a transfer task that may include a limited number of labels [3]. Early works in discriminative visual representation learning focused on training encoders to predict the position of an image patch [17, 41], predict the angle of rotation [21], and predict the colors in a grayscale image [67]. Current methods have shifted away from explicit rotation or color prediction, and instead, train an encoder to learn representations that are invariant to data augmentations [26, 8, 23, 9, 6, 45, 40]. This form of pretraining, known as instance discrimination pretraining, is often achieved through contrastive learning [43] or a teacher-student dual-network formulation[23]. The contrastive objective encourages representations from the

same image to be invariant to data augmentations and dissimilar to representations from other images (commonly referred to as negatives). Unlike contrastive objectives, Siamese representational learning methods do not rely on negatives and are thus less reliant on batch size [23, 9].

Region-Based and Object-Centric Self-Supervised Pretraining Instance discrimination pre-training has primarily focused on learning image-level representations. While this is suitable for downstream tasks such as image classification, learning local or object-centric features during pre-training is critical for tasks such as object detection and semantic segmentation. Recent works [56, 63, 60, 57, 31, 42, 2, 64, 61] have extended the instance discrimination paradigm to concurrently learn region-based features. These methods enforce representational invariance to image regions in both views without taking into consideration the content in these regions. Examples include DenseCL [56], which jointly trains the local features to be invariant across views while performing the standard image-level representation training, and ReSim [60], which performs region-level representation learning by sliding a window across the image regions present in both views and enforcing region-based representational similarity.

Xie et al. [63] go beyond simple feature-to-feature matching and incorporate spatial sensitivity when matching local features that are close in the embedding space. Our work extends region-based pretraining by refining small image regions into object-centric masks over training. Concurrent to this line of work are methods [28, 57, 2, 65, 53] that use heuristics to locate objects and enforce representational invariance for the features corresponding to these objects [19, 51]. The closest related work is DetCon [28], which uses unsupervised segmentation algorithms to train object-level representations. In contrast, our method is able to discover and represent objects by refining small image regions instead of relying on advanced segmentation heuristics to localize objects. Other works in this area [57, 53, 2, 65] focus on training object-centric features for a specific task, such as object detection, semantic segmentation, and salient object detection, and do not train a network to learn features that can transfer to multiple tasks. Concurrent to our work, Hénaff et al. [29] and Wen et al. [58] propose methods to directly discover objects, using K-means or learned semantic prototypes [37], and represent them without incorporating object-level heuristics or region-based pretraining.

Region Clustering In this work, we use clustering to refine small image regions into object-centric masks. Clustering has a long history in unsupervised semantic segmentation [19, 1, 16, 30, 14, 13]. This trend has continued in the era of deep learning. Current methods utilize clustering assignments in order to learn spatially and semantically consistent embeddings [35, 12, 32, 34]. Kanezaki [35], Hwang et al. [32] train pixelwise embeddings by clustering these embeddings and using the cluster assignments as pseudo labels. Cho et al. [12] and Ji et al. [34] train embedding using a similarity loss and task-specific data augmentations. Our work does not focus on the task of unsupervised semantic segmentation, and instead, focuses on using clustering to localize objects for learning transferable representations. Our method uses K-means clustering [36] due to its simplicity and effectiveness.

3 Method

We present *R2O*, a self-supervised pretraining method that enables region-level and object-centric representation learning. At a high level, *R2O* transforms region-level image priors into object-centric masks through a *region refinement module* and encourages representational invariance for the features corresponding to the contents of the discovered masks (see Figure 2). The training process begins by passing an image through the encoder as well as clustering the image into fine-grained regions using a simple algorithm such as SLIC [1]. Next, features for each region are pooled and clustered using K-means to create masks. A high number of clusters, K , leads to masks that group small image regions together. Conversely, we have found that using a lower number of clusters leads to neighboring image regions that are grouped together in order to form semantically meaningful segmentations which tend to correspond to objects. *R2O* then promotes representational similarity for the features corresponding to the refined masks, by aligning the features for refined regions across different views of the image. Finally, a region-to-object curriculum enables region-level and object-centric representation learning by gradually progressing masks from oversegmented regional fragments to accurate object-centric masks (Figure 1).

Formulation We formulate the pretraining objective as a bilevel optimization problem where the upper-level objective refines region-level priors into object-centric masks (Section 3.1) and the

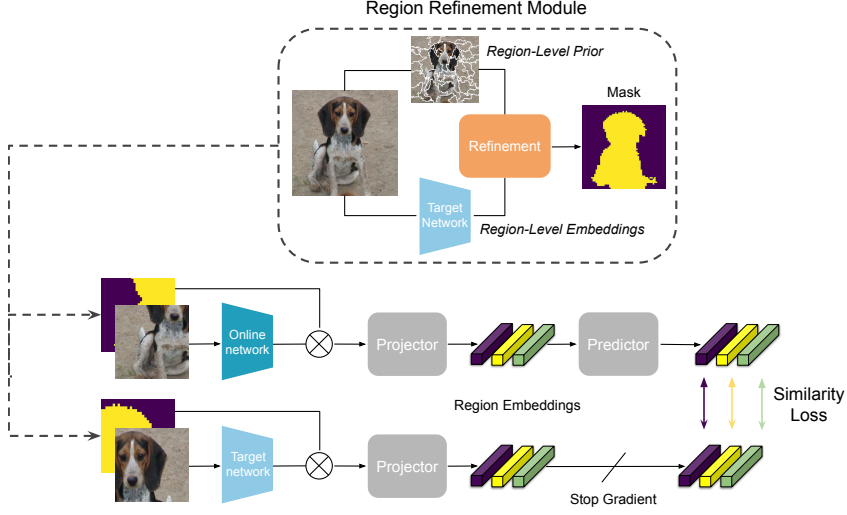


Figure 2: **R2O architecture.** *R2O* consists of two steps: (1) *Region Refinement*, where small image regions (given by a region-level prior) are transformed into object-centric masks and (2) *Representation Learning*, where object-level representations are learned. Step 1 produces object-centric segmentations by computing features for each region given by the region-level prior and performing K-means clustering on these region-level embeddings. Step 2 encourages representation similarity for the features corresponding to the refined mask in each view. *R2O* also uses a region-to-object curriculum which gradually decrease the number of clusters (K) during region refinement from a very high value ($K = 128$) to a low value ($K = 4$), which as we show, enables region-based pretraining early on during training and slowly evolves to object-centric pretraining.

lower-level objective optimizes representational invariance for mask-level features (Section 3.2). Let X refer to a given image and R be the region-level prior for the image (e.g. SLIC superpixels). The outer loop computes a cluster assignment, M , which is used to segment the image X , according to a mask-level objective ($\mathcal{L}_{\text{mask}}$) given the representation $f_{\theta}(X)$ and the region-level prior R (Eq. 1). The inner loop optimizes the parameters, θ , of the encoder, f_{θ} , following any representation learning objective ($\mathcal{L}_{\text{repr}}$) with respect to the segmentations created using M (Eq. 2).

$$\min_M \mathcal{L}_{\text{mask}}(M; f_{\theta^*}(X), R) \quad (1)$$

$$\text{s.t. } \theta^* = \underset{\theta}{\operatorname{argmin}} \mathcal{L}_{\text{repr}}(f_{\theta}(X); M) \quad (2)$$

3.1 Object-Centric Segmentation via Region Refinement

Our *Region Refinement* step refines a region-level prior, such as SLIC superpixels, into object-centric segmentations by clustering region-level features. Specifically, we define an object-centric segmentation as a set of clusters, M , which satisfy criteria such as color consistency, spatial proximity, and representational similarity. Region-level priors provide segmentations which satisfy image-level criteria, such as color consistency, and can be derived solely from a given image. However, as illustrated in Figure 2, these simple region-level priors do not accurately segment objects in the scene, but rather, group together small neighboring regions. Recent works have shown that representations learned from self-supervised pretraining can encode object-level semantics [66, 62, 52]. Thus, we incorporate the features learned during pretraining as part of our clustering objective in order to transform our region-level prior into object-centric segmentations.

We approximate the solution to the upper-level optimization problem (Eq. 1) by performing K-Means clustering on the set of region-level features to discover an object-centric segmentation. For each region, we compute an embedding, p_i , using a mask-pooling operation, where each region has a corresponding binary mask that selects the corresponding features in the convolutional feature map. This generates a set of region-level embeddings $P = \{p_1, \dots, p_{|R|}\}$ where $|R|$ is the number of

distinct regions generated by the region-level prior R . Next, we perform the refinement step shown in Figure 2 by applying K-Means clustering to the region-level embeddings in P in order to compute clusters $M = \{M_1, \dots, M_K\}$ (Eq. 3). Below, we denote $|M_i|$ as the number of points assigned to cluster M_i and μ_i is the mean of the points in M_i . Given cluster assignments M , we produce an object-centric segmentation, m , by assigning each pixel in the representation $f_\theta(X) \in \mathbb{R}^{H \times W \times D}$ to its nearest cluster center (see Mask in Figure 2).

$$\mathcal{L}_{\text{mask}}(M; f_\theta(X), R) = \frac{1}{K} \sum_{k=1}^K \frac{1}{|M_k|} \sum_{p \in M_k} \|p - \mu_k\|^2 \quad (3)$$

3.2 Object-Centric Representation Learning

Our representation learning process is similar to the BYOL pipeline [23]. Since optimizing this inner objective to convergence can be expensive, we approximate θ^* by minimizing $\mathcal{L}_{\text{repr}}(f_\theta(X); M)$ for one epoch using mini-batch gradient descent.

Setup Given an image X , we create two views: $x_1 = \mathcal{T}_{\text{aug}}(X)$, $x_2 = \mathcal{T}_{\text{aug}}(X)$, where \mathcal{T}_{aug} is any image augmentation policy. We use m to obtain m_1, m_2 corresponding to views x_1, x_2 . Further, we use a Siamese architecture with two similar networks: an online encoder f_θ (denoted by parameters θ) and a target encoder f_ξ (denoted by parameters ξ). The target network is not trained directly, and is updated using an exponential moving average of the online network’s parameters.

Pretraining We begin by computing $f_\theta(x_1), f_\xi(x_2) \in \mathbb{R}^{H \times W \times D}$. Next, we replace the commonly used global-pooling with mask-pooling [28]. This operation generates the average embeddings within the view-specific masks m_1 and m_2 . We compute $h_{\theta,1}$ and $h_{\xi,2}$ by applying mask-pooling to $f_{\theta,1}$ and $f_{\xi,2}$. Following the Siamese architecture, we compute $z_{\theta,1}$ and $z_{\xi,2}$ by forward-passing $h_{\theta,1}, h_{\xi,2}$ through the online network’s projector and the target network’s projector respectively. Finally, we forward-pass $z_{\theta,1}$ through the online network’s predictor to obtain $q_\theta(z_{\theta,1})$. We adopt the L2 loss according to the BYOL architecture (4). To make this loss symmetric for the view, we perform the same computation after swapping the two views to obtain $z_{\theta,2}, z_{\xi,1}$. Our final loss is provided in equation (5).

$$\mathcal{L}_{\text{BYOL}}(z_\theta, z_\xi) = 2 - 2 \cdot \frac{q_\theta(z_\theta) \cdot z_\xi}{\|q_\theta(z_\theta)\|_2 \cdot \|z_\xi\|_2} \quad (4)$$

$$\mathcal{L}_{\text{repr}} = \mathcal{L}_{\text{BYOL}}(z_{\theta,1}, z_{\xi,2}) + \mathcal{L}_{\text{BYOL}}(z_{\theta,2}, z_{\xi,1}) \quad (5)$$

3.3 Region-to-Object Curriculum

Empirically, we have found that varying the number of segments in the refined masks, from a high number to a low number, results in improved downstream performance and more accurate masks. Thus, we introduce a region-to-object curriculum which allows for *R2O* pretraining to learn both region based and object centric features. Specifically, we schedule the number of clusters K introduced in the region refinement step (Section 3.1). We have found that a region-to-object curriculum where K begins at a high value, e.g. $K = 128$, and is reduced to a low value, e.g. $K = 4$, over pretraining works best in terms of downstream performance. A visualization of the refined mask (Figure 1) illustrates how this curriculum allows for refined mask to become increasingly object centric (see Appendix A.8 for more examples). In this work, we explore a piecewise, linear, and cosine schedule for K .

4 Results

We evaluate *R2O* via common transfer learning paradigms by pretraining on the train set of the ImageNet ILSVRC-2012 dataset [48]. We evaluate representations when finetuned for object detection and instance segmentation on COCO and semantic segmentation on PASCAL VOC and Cityscapes. Furthermore, we perform several ablations exploring the various formulations and implementation

specifics of *R2O* discussed below. We also investigate unsupervised object segmentation on Caltech-UCSD Birds 200-2011 [55] using our ImageNet pretrained models. The license, PII, and consent details of each dataset are in the respective papers. We provide the code/models from this work at <https://github.com/KKallidromitis/r2o>.

Architecture We use a ResNet-50 [24] architecture for all encoders. Following, BYOL, all projector and predictions heads are 2 layer MLPs which use batch normalization [33] after the hidden layer. Our region refinement step uses the C4 output from our target network. For efficiency purposes, we perform K-means over the mini-batch on each GPU. Our refined mask m is of shape (14, 14). We use RoIAlign [25] to align m with views x_1 and x_2 . Our region-to-object representation learning step applies mask-pooling to the C5 output of the ResNet-50 similar to the existing use of global pooling.

Optimization We follow the optimization details of BYOL (full details in Supplementary A.1). Specifically, we use a base learning rate of 0.3, which is scaled linearly to batch size, and a weight decay of 10^{-6} . The learning rate is decayed by a cosine schedule after a warmup period which is one percent of the total pretraining time, e.g. 300 epochs of pretraining uses 3 warmup epochs. Our target network’s parameter τ , which details the tradeoff between the current parameters in the target and online networks, is increased over training following a cosine schedule. We use the LARS optimizer with a global batch size of 4096 distributed over 128 NVIDIA V100 GPUs. Our models are trained using PyTorch [44].

Refinement We generate 100 segments for each image using SLIC. We perform K-means with K initially set to 128. We use a cosine scheduler that decreases the value of K from 128 to 4 over the course of training. See Appendix A.1 for additional experimental details.

4.1 Transfer Learning Details

Object Detection and Instance Segmentation: MS COCO We finetune our encoder as the backbone of a Mask-RCNN (R50-FPN) [25] using Detectron2 [59]. We follow the $1\times$ (12 epochs) and $2\times$ (24 epochs) training schedule, training on MS COCO’s train2017 dataset and evaluating on the val2017 dataset. We report average precision for bounding box predictions (AP_{bb}) and mask predictions (AP_{mk}). Hyperparameter details and variance across multiple random seeds are reported in Appendix A.1.

Semantic Segmentation: PASCAL VOC and Cityscapes. We evaluate our semantic segmentation performance by finetuning the encoder as the backbone of a FCN [38] using MMSegmentation [15]. For PASCAL VOC, we finetune using the train_aug2012 dataset for 45 epochs. For Cityscapes, we finetune using the train_fine dataset for 160 epochs. Our evaluation pipeline follows the architecture and hyperparameters found in He et al. [26]. Performance is measured by mean intersection-over-union (mIOU) on val2012 and val_fine respectively. To ensure fair comparison [22], we tune the hyperparameters used in evaluation for all related methods. Full details regarding hyperparameters and standard deviation of performance over random trials are in Appendix A.3.

4.2 ImageNet-1K Transfer

We use the BYOL data augmentation policy to generate two views during pretraining which lasts for 300 epochs. Additionally, we compute SLIC masks using a 224×224 resized version of the original image.

Object Detection and Instance Segmentation Table 1 shows our performance on COCO object detection and instance segmentation. Our method outperforms state-of-the-art methods when using the $1\times$ schedule ($+0.2 AP_{bb}$, $+0.3 AP_{mk}$) and is competitive with these methods when using the $2\times$ schedule ($+0.1 AP_{bb}$, $+0.1 AP_{mk}$). We attribute our state-of-the-art performance on instance segmentation to the nature of our pretraining. *R2O* segments a scene by refining a large number of small regions based on image-level priors to a few larger regions that are semantically meaningful using learned representations while learning representations corresponding to each of the discovered segments. Thus, segmentation based tasks should benefit from this form of pretraining process as

Method	COCO 1×		COCO 2×	
	AP ^{bb}	AP ^{mk}	AP ^{bb}	AP ^{mk}
Supervised	38.9	35.4	40.6	36.8
MoCo v2 [10]	38.9	35.4	40.9	37.0
BYOL [†] [23]	40.6	37.5	42.0	38.7
DenseCL [56]	40.3	36.4	41.2	37.3
ReSim [60]	39.3	35.7	41.1	37.1
PixPro [63]	41.4	-	-	-
DetCon _B [†] [28]	41.5	38.0	42.1	38.9
DetCo [61]	39.4	34.4	41.4	35.8
LEWEL [31]	41.3	37.4	42.2	38.2
<i>R2O</i>	41.7	38.3	42.3	39.0

Table 1: **Performance on COCO object detection and instance segmentation following ImageNet pretraining.** All methods pretrained a ResNet-50 which later served as the backbone of a Mask R-CNN R50-FPN finetuned on train2017 for 12 epochs (1× schedule) or 24 epochs (2× schedule). We report Average Precision on bounding box (AP^{bb}) and mask (AP^{mk}) predictions for val2017. [†]: Results from re-implementation.

representations learned during pretraining rely upon the boundaries of the discovered masks instead of rectangular bounding boxes.

Semantic Segmentation As seen in Table 2, we outperform existing methods on PASCAL VOC (+0.7 mIOU) and Cityscapes (+0.4 mIOU) semantic segmentation. We believe our improvements in semantic segmentation demonstrate the benefits of pretraining region-level and object-centric representations. *R2O* improves transfer performance on this task as pixel-level features are learned while also training the object-centric representations needed to identify the objects in the scene. In particular, the benefits of *R2O* is demonstrated by our state-of-the-art performance on the PASCAL VOC semantic segmentation task, a pixel-level classification task which is object-focused as most of its classes are also present in ImageNet-1K.

Method	PASCAL VOC	Cityscapes
Supervised	72.4	74.7
MoCo v2 [10]	73.9	75.6
BYOL [†] [23]	75.0	75.8
DenseCL [56]	73.8	76.1
DetCon _B [†] [28]	76.0	76.2
ReSim [60]	74.3	75.5
PixPro [63]	74.2	75.9
DetCo [61]	74.3	74.9
LEWEL [31]	75.5	75.4
<i>R2O</i>	76.7	76.6

Table 2: **Performance on PASCAL VOC and Cityscapes semantic segmentation (mIOU) following ImageNet pretraining.** Unless otherwise stated, results are computing using pretrained weights officially released by the authors. [†]: Results from re-implementation of pretraining method.

4.3 Unsupervised Object Segmentation

We investigate the quality of segmentations from *R2O* pretrained features by evaluating unsupervised object segmentation on Caltech-UCSD Birds 200-2011 (CUB-200-2011). We use our ImageNet pretrained ResNet-50 and generate object segmentations by applying K-means clustering to image features with $K = 5$. We use Hungarian matching to assign one segment as the foreground and the rest segments are considered as background. This approach accounts for the high variance in

the background (e.g., trees, ground, sky, etc.). Table 3 shows our performance, measured by mean intersection-over-union (mIOU), when segmenting the foreground and background on a test from CUB-200-2011 used in prior works [7]. Table 3 also provides self-supervised pretrained baselines using MoCo v2 [10] and BYOL [23] following our evaluation protocol. In comparison to existing unsupervised object segmentation methods [5, 7, 4, 54], segmentation via K-means clustering of *R2O* pretrained ResNet-50 features surpasses state-of-the-art (+2.9 mIOU) *without finetuning on CUB-200-2011*. Similar to our protocol, Melas-Kyriazi et al. [39] extract accurate segmentations from ImageNet pretrained GANs, without finetuning on CUB-200-2011, in order to train a UNet [47]. *R2O* outperforms Melas-Kyriazi et al. [39] (+4.8 mIOU) using only K-means clustering on features from *R2O* pretrained encoders.

Method	CUB-200-2011
<i>Self-Supervised Pretraining Methods</i>	
MoCo v2 [10]	63.5
BYOL [†] [23]	65.1
<i>Unsupervised Object Segmentation Methods</i>	
PerturbGAN [5]	38.0
ReDO [7]	42.6
OneGAN [4]	55.5
Voynov et al. [54]	68.3
Melas-Kyriazi et al. [39]	66.4
<i>R2O</i>	71.2

Table 3: **Performance on CUB-200-2011 segmentation.** Results report the mean intersection-over-union (mIOU) for foreground-background segmentations of images in a Caltech-UCSD Birds 200-2011 (CUB-200-2011) test set [7]. Unlike [5, 7, 4, 54], we are able to produce state-of-the-art quality segmentations (+2.9 mIOU) using our ImageNet pretrained encoder and *without finetuning on CUB-200-2011*. [†]: Results from re-implementation.

4.4 Ablation and Analysis

To examine the importance of region-to-object pretraining, we experiment with different schedule types. Furthermore, we also evaluate the effectiveness of our region refinement module. The models used in these ablations are pretrained on ImageNet100 [50] for 100 epochs and evaluated on PASCAL VOC semantic segmentation using the details in Section 4.1. We provide ablations on the effect of the type of scheduler (e.g. cosine, linear, piecewise) and type of neighborhood prior (SLIC versus spatial segmentation) in the Appendix (A.6, A.7). The Appendix also includes ablations examining the use of a contrastive representation learning objective (Appendix A.4) and transfer performance when using a Vision Transformer (ViT) encoder [18] (Appendix A.5).

Quantifying objectness of the masks throughout pretraining. We use the Average Best Overlap (ABO) [51] to measure the improvement of masks throughout training using semantic segmentation annotations for ImageNet-1K provided by LUSS [20]. As shown in Figure 3, our ABO improved by 0.25 over the course of pretraining. As a reference, Figure 3 includes the ABO of our SLIC prior as well. Masks refined by *R2O* are consistently better than SLIC segments, suggesting that the refinement step is able to improve small region priors into more object-like masks that are semantically meaningful.

Evaluating Alternate Schedules. Table 4 demonstrates that a region-to-object schedule leads to the best transfer performance on PASCAL VOC (+1.2 mIOU) for semantic segmentation. This schedule outperforms using a fixed K and an opposite schedule which increases K from a low value to a high value. Using a fixed K does not allow for learning both region based features, corresponding to image patches without objects, and object centric representation learning. If the fixed value of K is high, say $K = 64$, then refined masks will have many distinct regions and the representation learning step will train features corresponding to small image regions or object parts. A small fixed value of K , say $K = 4$, has the opposite effect as representations learned will simply match large image

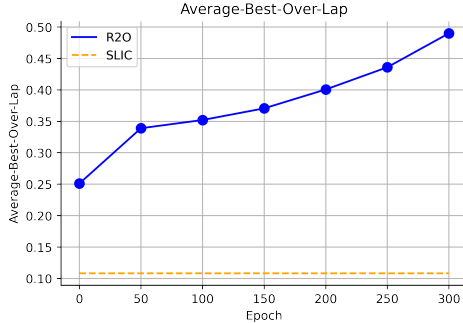


Figure 3: ***R2O* refined masks become increasingly object-centric over pretraining.** We compute average best overlap (ABO) for ImageNet segmentations (using LUSS annotations) generated over the course of pretraining. For reference, we also display the ABO of our region-level prior (SLIC).

Schedule		PASCAL VOC (mIOU)
reg \rightarrow obj	16 \rightarrow 4	61.1
	64 \rightarrow 4	61.5
	128 \rightarrow 4	62.3
	256 \rightarrow 4	61.7
obj \rightarrow reg	4 \rightarrow 16	60.2
	4 \rightarrow 64	60.8
	4 \rightarrow 128	61.0
	4 \rightarrow 256	61.1

Table 4: **Comparing region-to-object, object-to-region, and fixed K curriculum.** We pre-train an encoder on ImageNet100 while using alternate schedules for our region refinement step. We report mean intersection-over-union (mIOU) after finetuning on PASCAL VOC semantic segmentation.

regions across views and cannot learn small region based features necessary for pixel level prediction tasks. The opposite schedule, denoted as object-to-region, also leads to suboptimal performance. We believe this is because such a schedule does not allow for objects to be found and represented. Instead, early refined masks are just large image regions without any semantic meaning as the network has undergone very little training.

Region Refinement	SLIC Prior	Region-to-Object Schedule	PASCAL VOC (mIOU)
\times	\times	\times	61.2
\checkmark	\times	\times	61.5
\times	\times	\checkmark	61.4
\checkmark	\times	\checkmark	61.5
\times	\checkmark	\checkmark	61.7
\checkmark	\checkmark	\times	61.4
\checkmark	\checkmark	\checkmark	62.3

Table 5: **Importance of *R2O* components.** We ablate the key components of the *R2O* pretraining process, namely: the region refinement module, the use of a prior (SLIC), and the region-to-object schedule. As shown, the combination of using Region Refinement, SLIC Prior, and Region-to-Object Schedule are necessary for the top performing result (62.3 mIOU) – removing any component decreases performance by at least 0.6 mIOU.

Effect of of Region Refinement Table 5 details the results of ablating each key component in *R2O* pretraining. The baseline method, which does not use a SLIC prior, region-to-object schedule, nor the region refinemet, performs the worst. This baseline method is a region-to-region form of pretraining, similar to DenseCL [56] but without the method’s feature matching strategy. We find that our Region-to-Object Schedule has the largest impact on performance (+0.9 mIOU) because this element combines the region level learning and object level learning. Moreover, Table 5 shows that the combination of using Region Refinement, SLIC Prior, and Region-to-Object Schedule are necessary for the top performing result (62.3 mIOU); removing any component decreases performance.

Limitations While our experiments and ablations indicate that *R2O* learns object-centric masks throughout pretraining, we do not have a guarantee that such masks will necessarily identify objects. As shown by several examples in Appendix A.8, there are several failure cases where *R2O* segmentations group different objects together or separates parts of objects that have significantly different color, texture, or brightness compared to the rest of the object. *R2O* is an unsupervised pretraining algorithm, and without semantic grounding from object-level annotations, it cannot

necessarily distinguish between the semantics of what constitutes an object. Nevertheless, as indicated by our strong experimental results, *R2O* learns useful representations that can be finetuned for dense downstream prediction tasks.

5 Conclusion

We present Region-to-Object Representation Learning (*R2O*) which unifies region-based and object-centric instance pretraining by learning both region-level and object-centric representations using only simple region-level priors. While existing methods have either focused exclusively on region-based or object-centric pretraining, *R2O* shows that a region-to-object curriculum which transitions between these two objectives leads to strong representations for a variety of downstream tasks such as detection and segmentation. Furthermore, we have found *R2O* pretraining generates object-centric segmentations during pretraining and our ImageNet pretrained encoders establish new state-of-the-art in unsupervised object segmentations on different downstream datasets.

6 Broader Impacts and Acknowledgements

Our method can learn object-centric features using unsupervised pretraining. As demonstrated in Section 4, this can benefit downstream tasks such as object detection and segmentation. However, *R2O* does not guarantee the output of object-centric masks. Thus, representations learned using *R2O* could exhibit the negative artifacts seen in image-level pretraining, such as only focusing on background pixels [49]. Caution must be exercised in safety-critical applications of our method.

Acknowledgements: We thank Tete Xiao for valuable discussions and feedback. This work was supported in part by DoD including DARPA’s LwLL, PTG and/or SemaFor programs, as well as BAIR’s industrial alliance programs. We thank the authors of DetCon [28] for assisting us with reproducing their baselines.

References

- [1] R. Achanta, A. Shaji, K. Smith, A. Lucchi, P. Fua, and S. Süsstrunk. Slic superpixels compared to state-of-the-art superpixel methods. *IEEE transactions on pattern analysis and machine intelligence*, 34(11):2274–2282, 2012. (Cited on 3)
- [2] A. Bar, X. Wang, V. Kantorov, C. J. Reed, R. Herzig, G. Chechik, A. Rohrbach, T. Darrell, and A. Globerson. Detreg: Unsupervised pretraining with region priors for object detection. *arXiv preprint arXiv:2106.04550*, 2021. (Cited on 1, 3)
- [3] Y. Bengio, A. Courville, and P. Vincent. Representation learning: A review and new perspectives. *IEEE transactions on pattern analysis and machine intelligence*, 35(8):1798–1828, 2013. (Cited on 2)
- [4] Y. Benny and L. Wolf. Onegan: Simultaneous unsupervised learning of conditional image generation, foreground segmentation, and fine-grained clustering. In *European Conference on Computer Vision*, pages 514–530. Springer, 2020. (Cited on 8)
- [5] A. Bielski and P. Favaro. Emergence of object segmentation in perturbed generative models. *Advances in Neural Information Processing Systems*, 32, 2019. (Cited on 8)
- [6] M. Caron, H. Touvron, I. Misra, H. Jégou, J. Mairal, P. Bojanowski, and A. Joulin. Emerging properties in self-supervised vision transformers. In *Proceedings of the IEEE/CVF International Conference on Computer Vision*, pages 9650–9660, 2021. (Cited on 1, 2, 17)
- [7] M. Chen, T. Artières, and L. Denoyer. Unsupervised object segmentation by redrawing. *Advances in neural information processing systems*, 32, 2019. (Cited on 8)
- [8] T. Chen, S. Kornblith, M. Norouzi, and G. Hinton. A simple framework for contrastive learning of visual representations. In *International conference on machine learning*, pages 1597–1607. PMLR, 2020. (Cited on 1, 2, 16)
- [9] X. Chen and K. He. Exploring simple siamese representation learning. In *Proceedings of the IEEE/CVF Conference on Computer Vision and Pattern Recognition*, pages 15750–15758, 2021. (Cited on 2, 3)
- [10] X. Chen, H. Fan, R. Girshick, and K. He. Improved baselines with momentum contrastive learning. *arXiv preprint arXiv:2003.04297*, 2020. (Cited on 7, 8, 16)
- [11] X. Chen, S. Xie, and K. He. An empirical study of training self-supervised vision transformers. In *Proceedings of the IEEE/CVF International Conference on Computer Vision*, pages 9640–9649, 2021. (Cited on 17)
- [12] J. H. Cho, U. Mall, K. Bala, and B. Hariharan. Picie: Unsupervised semantic segmentation using invariance and equivariance in clustering. In *Proceedings of the IEEE/CVF Conference on Computer Vision and Pattern Recognition*, pages 16794–16804, 2021. (Cited on 3)
- [13] D. Comaniciu and P. Meer. Robust analysis of feature spaces: Color image segmentation. In *Proceedings of IEEE computer society conference on computer vision and pattern recognition*, pages 750–755. IEEE, 1997. (Cited on 3)
- [14] D. Comaniciu and P. Meer. Mean shift analysis and applications. In *Proceedings of the seventh IEEE international conference on computer vision*, volume 2, pages 1197–1203. IEEE, 1999. (Cited on 3)
- [15] M. Contributors. MMSegmentation: Openmmlab semantic segmentation toolbox and benchmark. <https://github.com/open-mmlab/mms Segmentation>, 2020. (Cited on 6, 15)
- [16] N. Dhanachandra, K. Manglem, and Y. J. Chanu. Image segmentation using k-means clustering algorithm and subtractive clustering algorithm. *Procedia Computer Science*, 54:764–771, 2015. (Cited on 3)
- [17] C. Doersch, A. Gupta, and A. A. Efros. Unsupervised visual representation learning by context prediction. In *Proceedings of the IEEE international conference on computer vision*, pages 1422–1430, 2015. (Cited on 2)
- [18] A. Dosovitskiy, L. Beyer, A. Kolesnikov, D. Weissenborn, X. Zhai, T. Unterthiner, M. Dehghani, M. Minderer, G. Heigold, S. Gelly, et al. An image is worth 16x16 words: Transformers for image recognition at scale. *arXiv preprint arXiv:2010.11929*, 2020. (Cited on 8, 17)
- [19] P. F. Felzenszwalb and D. P. Huttenlocher. Efficient graph-based image segmentation. *International journal of computer vision*, 59(2):167–181, 2004. (Cited on 3)

- [20] S.-H. Gao, Z.-Y. Li, M.-H. Yang, M.-M. Cheng, J. Han, and P. Torr. Large-scale unsupervised semantic segmentation. *arXiv preprint arXiv:2106.03149*, 2021. (Cited on 8)
- [21] S. Gidaris, P. Singh, and N. Komodakis. Unsupervised representation learning by predicting image rotations. *arXiv preprint arXiv:1803.07728*, 2018. (Cited on 2)
- [22] P. Goyal, D. Mahajan, A. Gupta, and I. Misra. Scaling and benchmarking self-supervised visual representation learning. In *Proceedings of the IEEE/CVF International Conference on computer vision*, pages 6391–6400, 2019. (Cited on 6, 16)
- [23] J.-B. Grill, F. Strub, F. Altché, C. Tallec, P. Richemond, E. Buchatskaya, C. Doersch, B. Avila Pires, Z. Guo, M. Gheshlaghi Azar, et al. Bootstrap your own latent—a new approach to self-supervised learning. *Advances in Neural Information Processing Systems*, 33: 21271–21284, 2020. (Cited on 2, 3, 5, 7, 8, 15, 16)
- [24] K. He, X. Zhang, S. Ren, and J. Sun. Deep residual learning for image recognition. In *Proceedings of the IEEE conference on computer vision and pattern recognition*, pages 770–778, 2016. (Cited on 6)
- [25] K. He, G. Gkioxari, P. Dollár, and R. Girshick. Mask r-cnn. In *Proceedings of the IEEE international conference on computer vision*, pages 2961–2969, 2017. (Cited on 6, 15)
- [26] K. He, H. Fan, Y. Wu, S. Xie, and R. Girshick. Momentum contrast for unsupervised visual representation learning. In *Proceedings of the IEEE/CVF conference on computer vision and pattern recognition*, pages 9729–9738, 2020. (Cited on 2, 6, 15)
- [27] K. He, X. Chen, S. Xie, Y. Li, P. Dollár, and R. Girshick. Masked autoencoders are scalable vision learners. In *Proceedings of the IEEE/CVF Conference on Computer Vision and Pattern Recognition*, pages 16000–16009, 2022. (Cited on 17)
- [28] O. J. Hénaff, S. Koppula, J.-B. Alayrac, A. van den Oord, O. Vinyals, and J. Carreira. Efficient visual pretraining with contrastive detection. In *Proceedings of the IEEE/CVF International Conference on Computer Vision*, pages 10086–10096, 2021. (Cited on 1, 3, 5, 7, 10, 16)
- [29] O. J. Hénaff, S. Koppula, E. Shelhamer, D. Zoran, A. Jaegle, A. Zisserman, J. Carreira, and R. Arandjelović. Object discovery and representation networks. *arXiv preprint arXiv:2203.08777*, 2022. (Cited on 3)
- [30] J. Hou, H. Gao, and X. Li. Dsets-dbscan: A parameter-free clustering algorithm. *IEEE Transactions on Image Processing*, 25(7):3182–3193, 2016. (Cited on 3)
- [31] L. Huang, S. You, M. Zheng, F. Wang, C. Qian, and T. Yamasaki. Learning where to learn in cross-view self-supervised learning. *arXiv preprint arXiv:2203.14898*, 2022. (Cited on 3, 7, 16)
- [32] J.-J. Hwang, S. X. Yu, J. Shi, M. D. Collins, T.-J. Yang, X. Zhang, and L.-C. Chen. Segsort: Segmentation by discriminative sorting of segments. In *Proceedings of the IEEE/CVF International Conference on Computer Vision*, pages 7334–7344, 2019. (Cited on 3)
- [33] S. Ioffe and C. Szegedy. Batch normalization: Accelerating deep network training by reducing internal covariate shift. In *Proceedings of the 32nd International Conference on Machine Learning*, Proceedings of Machine Learning Research. PMLR, 2015. (Cited on 6)
- [34] X. Ji, J. F. Henriques, and A. Vedaldi. Invariant information clustering for unsupervised image classification and segmentation. In *Proceedings of the IEEE/CVF International Conference on Computer Vision*, pages 9865–9874, 2019. (Cited on 3)
- [35] A. Kanezaki. Unsupervised image segmentation by backpropagation. In *2018 IEEE international conference on acoustics, speech and signal processing (ICASSP)*, pages 1543–1547. IEEE, 2018. (Cited on 3)
- [36] S. Lloyd. Least squares quantization in pcm. *IEEE transactions on information theory*, 28(2): 129–137, 1982. (Cited on 3)
- [37] F. Locatello, D. Weissenborn, T. Unterthiner, A. Mahendran, G. Heigold, J. Uszkoreit, A. Dosovitskiy, and T. Kipf. Object-centric learning with slot attention. *Advances in Neural Information Processing Systems*, 33:11525–11538, 2020. (Cited on 3)
- [38] J. Long, E. Shelhamer, and T. Darrell. Fully convolutional networks for semantic segmentation. In *Proceedings of the IEEE conference on computer vision and pattern recognition*, pages 3431–3440, 2015. (Cited on 6, 15)

- [39] L. Melas-Kyriazi, C. Rupprecht, I. Laina, and A. Vedaldi. Finding an unsupervised image segmenter in each of your deep generative models. *arXiv preprint arXiv:2105.08127*, 2021. (Cited on 8)
- [40] I. Misra and L. v. d. Maaten. Self-supervised learning of pretext-invariant representations. In *Proceedings of the IEEE/CVF Conference on Computer Vision and Pattern Recognition*, pages 6707–6717, 2020. (Cited on 2)
- [41] M. Noroozi and P. Favaro. Unsupervised learning of visual representations by solving jigsaw puzzles. In *European conference on computer vision*, pages 69–84. Springer, 2016. (Cited on 2)
- [42] P. O. O. Pinheiro, A. Almahairi, R. Benmalek, F. Golemo, and A. C. Courville. Unsupervised learning of dense visual representations. *Advances in Neural Information Processing Systems*, 33:4489–4500, 2020. (Cited on 3)
- [43] A. v. d. Oord, Y. Li, and O. Vinyals. Representation learning with contrastive predictive coding. *arXiv preprint arXiv:1807.03748*, 2018. (Cited on 2)
- [44] A. Paszke, S. Gross, F. Massa, A. Lerer, J. Bradbury, G. Chanan, T. Killeen, Z. Lin, N. Gimelshein, L. Antiga, A. Desmaison, A. Kopf, E. Yang, Z. DeVito, M. Raison, A. Tejani, S. Chilamkurthy, B. Steiner, L. Fang, J. Bai, and S. Chintala. Pytorch: An imperative style, high-performance deep learning library. In H. Wallach, H. Larochelle, A. Beygelzimer, F. d'Alché-Buc, E. Fox, and R. Garnett, editors, *Advances in Neural Information Processing Systems 32*, pages 8024–8035. Curran Associates, Inc., 2019. URL <http://papers.neurips.cc/paper/9015-pytorch-an-imperative-style-high-performance-deep-learning-library.pdf>. (Cited on 6)
- [45] C. J. Reed, S. Metzger, A. Srinivas, T. Darrell, and K. Keutzer. Selfaugment: Automatic augmentation policies for self-supervised learning. In *Proceedings of the IEEE/CVF Conference on Computer Vision and Pattern Recognition (CVPR)*, pages 2674–2683, June 2021. (Cited on 2)
- [46] C. J. Reed, X. Yue, A. Nrusimha, S. Ebrahimi, V. Vijaykumar, R. Mao, B. Li, S. Zhang, D. Guillory, S. Metzger, K. Keutzer, and T. Darrell. Self-supervised pretraining improves self-supervised pretraining. In *Proceedings of the IEEE/CVF Winter Conference on Applications of Computer Vision (WACV)*, pages 2584–2594, January 2022. (Cited on 1)
- [47] O. Ronneberger, P. Fischer, and T. Brox. U-net: Convolutional networks for biomedical image segmentation. In *International Conference on Medical image computing and computer-assisted intervention*, pages 234–241. Springer, 2015. (Cited on 8)
- [48] O. Russakovsky, J. Deng, H. Su, J. Krause, S. Satheesh, S. Ma, Z. Huang, A. Karpathy, A. Khosla, M. Bernstein, et al. Imagenet large scale visual recognition challenge. *International journal of computer vision*, 115(3):211–252, 2015. (Cited on 5)
- [49] R. R. Selvaraju, K. Desai, J. Johnson, and N. Naik. Casting your model: Learning to localize improves self-supervised representations. In *Proceedings of the IEEE/CVF Conference on Computer Vision and Pattern Recognition*, pages 11058–11067, 2021. (Cited on 10)
- [50] Y. Tian, D. Krishnan, and P. Isola. Contrastive multiview coding. *arXiv preprint arXiv:1906.05849*, 2019. (Cited on 8)
- [51] J. R. Uijlings, K. E. Van De Sande, T. Gevers, and A. W. Smeulders. Selective search for object recognition. *International journal of computer vision*, 104(2):154–171, 2013. (Cited on 3, 8)
- [52] W. Van Gansbeke, S. Vandenhende, S. Georgoulis, M. Proesmans, and L. Van Gool. Scan: Learning to classify images without labels. In *European conference on computer vision*, pages 268–285. Springer, 2020. (Cited on 4)
- [53] W. Van Gansbeke, S. Vandenhende, S. Georgoulis, and L. Van Gool. Unsupervised semantic segmentation by contrasting object mask proposals. In *Proceedings of the IEEE/CVF International Conference on Computer Vision*, pages 10052–10062, 2021. (Cited on 3)
- [54] A. Voynov, S. Morozov, and A. Babenko. Object segmentation without labels with large-scale generative models. In *International Conference on Machine Learning*, pages 10596–10606. PMLR, 2021. (Cited on 8)
- [55] C. Wah, S. Branson, P. Welinder, P. Perona, and S. Belongie. The caltech-ucsd birds-200-2011 dataset. 2011. (Cited on 6)

- [56] X. Wang, R. Zhang, C. Shen, T. Kong, and L. Li. Dense contrastive learning for self-supervised visual pre-training. In *Proceedings of the IEEE/CVF Conference on Computer Vision and Pattern Recognition*, pages 3024–3033, 2021. (Cited on 1, 3, 7, 9, 16)
- [57] F. Wei, Y. Gao, Z. Wu, H. Hu, and S. Lin. Aligning pretraining for detection via object-level contrastive learning. *Advances in Neural Information Processing Systems*, 34, 2021. (Cited on 1, 3)
- [58] X. Wen, B. Zhao, A. Zheng, X. Zhang, and X. Qi. Self-supervised visual representation learning with semantic grouping. *arXiv preprint arXiv:2205.15288*, 2022. (Cited on 3)
- [59] Y. Wu, A. Kirillov, F. Massa, W.-Y. Lo, and R. Girshick. Detectron2. <https://github.com/facebookresearch/detectron2>, 2019. (Cited on 6)
- [60] T. Xiao, C. J. Reed, X. Wang, K. Keutzer, and T. Darrell. Region similarity representation learning. In *Proceedings of the IEEE/CVF International Conference on Computer Vision*, pages 10539–10548, 2021. (Cited on 1, 3, 7, 16)
- [61] E. Xie, J. Ding, W. Wang, X. Zhan, H. Xu, P. Sun, Z. Li, and P. Luo. Detco: Unsupervised contrastive learning for object detection. In *Proceedings of the IEEE/CVF International Conference on Computer Vision*, pages 8392–8401, 2021. (Cited on 3, 7, 16)
- [62] J. Xie, X. Zhan, Z. Liu, Y. S. Ong, and C. C. Loy. Unsupervised object-level representation learning from scene images. *Advances in Neural Information Processing Systems*, 34:28864–28876, 2021. (Cited on 4)
- [63] Z. Xie, Y. Lin, Z. Zhang, Y. Cao, S. Lin, and H. Hu. Propagate yourself: Exploring pixel-level consistency for unsupervised visual representation learning. In *Proceedings of the IEEE/CVF Conference on Computer Vision and Pattern Recognition*, pages 16684–16693, 2021. (Cited on 1, 3, 7, 16)
- [64] Y. Xu, Q. Zhang, J. Zhang, and D. Tao. Regioncl: Can simple region swapping contribute to contrastive learning? *arXiv preprint arXiv:2111.12309*, 2021. (Cited on 3)
- [65] C. Yang, L. Huang, and E. J. Crowley. Contrastive object-level pre-training with spatial noise curriculum learning. *arXiv preprint arXiv:2111.13651*, 2021. (Cited on 1, 3)
- [66] F. Zhang, P. Torr, R. Ranftl, and S. Richter. Looking beyond single images for contrastive semantic segmentation learning. *Advances in Neural Information Processing Systems*, 34, 2021. (Cited on 4)
- [67] R. Zhang, P. Isola, and A. A. Efros. Colorful image colorization. In *European conference on computer vision*, pages 649–666. Springer, 2016. (Cited on 2)

Appendix

A.1 Pretraining Details

Data Augmentation We follow the BYOL [23] data augmentation pipeline. The SLIC masks are generated using a resized copy of the input image. To generate the augmented views, we implement the following operations using `torchvision`.

1. Random Crop: Generate two distinct random crops from the original image. Afterwards we resize both views to 224×224 .
2. Horizontal Flip: We flip the views horizontally with a 0.5 probability.
3. Color Jitter: With an implementation probability of 0.8 we set brightness equal to 0.4, contrast = 0.4, saturation = 0.2 and hue = 0.1.
4. Grayscale: We convert the images from RGB to Grayscale with a 0.2 probability.
5. Gaussian Blur: We always apply blurring for the first view and with a 0.1 probability for the second view. We use a 23×23 kernel with a standard deviation chosen uniformly at random between ranges $[0.1, 2.0]$.
6. Solarize: Solarize only implemented on view 2 with a probability of 0.2 using the PIL package and a threshold of 128.

Refinement We employ a cosine schedule for the number of segments, K , which starts at K_0 at epoch 0 and gradually decreases to K_f between epoch t_α and T_{epoch} , where T_{epoch} is the total number of epochs during the pretraining. Equation A1 expresses K as a function of t , the epoch number. We choose $K_0 = 128$, $K_f = 4$, $t_\alpha = 40$, $T_{epoch} = 300$ in our experiment.

$$K(t) = \begin{cases} K_0, & \text{if } t < t_\alpha \\ K_f + \cos\left(\frac{2(t-t_\alpha)}{(T_{epoch}-t_\alpha)\cdot\pi}\right)(K_0 - K_f) & \text{otherwise} \end{cases} \quad (\text{A1})$$

Optimization We followed BYOL [23] optimization. The online network is updated by a LARS optimizer with a base learning rate of 0.3 and a weight decay of 10^{-6} . The actual maximum learning rate during training is $\text{base_lr} \times \frac{\text{global_batch_size}}{256}$. The learning rate increases linearly during the warmup period and then decreases following a cosine schedule. In our experiment, the global batch size is 4096 and the warmup period is 3 epochs. The target network parameter ξ is updated by $\xi^t \leftarrow (1 - \tau^t) \cdot \theta^t + \tau^t \cdot \xi^{t-1}$ where θ is the online network parameter and τ increases from 0.99 to 1.00 following a cosine schedule.

A.2 Transfer Learning Details

Object Detection and Instance Segmentation: MS COCO We adopt Mask-RCNN [25] architecture with a ResNet-50 backbone and FPN. In the fine tuning stage, images are randomly flipped and resized to $u \cdot 1024$ on the longest side where u is uniformly sampled in $[0.8, 1.25]$. The images are then padded or cropped to 1024×1024 . The aspect ratio is kept the same as original image. During the evaluation, the images are resized to 1024 on the longest side. We fine tuned on COCO for the $1\times$ and $2\times$ schedule using stochastic gradient descent. We swept between learning rates of 0.003, 0.1, 0.3 for our model and our DetCon implementation to ensure a fair comparison. We use a momentum of 0.9, a weight decay of $4 \cdot 10^{-5}$, and a global batch size of 32. The learning rate increases linearly in the first 1000 epochs and drops twice by a factor of 10 after $\frac{2}{3}$ and $\frac{8}{9}$ of the total training time.

Semantic Segmentation: PASCAL VOC and Cityscapes We adopt FCN [38] architecture with a ResNet-50 backbone. We made the following architecture changes on the backbone according to MOCO [26]. The 3×3 convolutions in conv5 blocks have dilation 2 and stride 1. This is followed by two extra 3×3 convolutions of 256 channels with BN and ReLU, and then a 1×1 convolution for per-pixel classification. We set dilation = 6 in the two extra 3×3 convolutions. All other implementation details are the default of MMSegmentation [15]. For PASCAL VOC, we fine tuned on train_aug2012

and evaluated on val2012 dataset. The images are randomly flipped, scaled by a ratio randomly sampled in $[0.5, 2.0]$, and then cropped to 513×513 during the training. The evaluation is performed on the original image size. We fine tuned for 30k iterations with a batch size of 16 and a weight decay of 10^{-4} . The learning rate is dropped by a factor of 10 at $\frac{7}{10}$ and $\frac{9}{10}$ of the total training time. For Cityscapes, we fine tuned on train_fine and evaluated on val_fine dataset. The images are randomly flipped, resized to 2049×1025 , scaled by a ratio randomly sampled in $[0.5, 2.0]$, and then cropped to 769×769 during the training. The evaluation is performed on a resolution of 2049×1025 . We fine tuned for 30k iterations with a batch size of 16, and a weight decay of 10^{-4} . The learning rate is dropped by a factor of 10 at $\frac{7}{10}$ and $\frac{9}{10}$ of the total training time. To ensure a fair comparison, we followed the practice of [22] and evaluate each pretraining method under a variety of learning rates and report the best results. We also report the standard deviation across three random seeds. For PASCAL VOC, we swept between the learning rate 0.001, 0.003, 0.01, 0.03, 0.1. For Cityscapes, we swept between learning rate 0.004, 0.01, 0.04.

A.3 Extended Experimental Results

We conduct additional experiments and report the average performance on semantic segmentation and instance detection/segmentation with standard deviation across 3 different seeds in table A1 and A2.

Method	PASCAL VOC	Cityscapes
Supervised	72.4	74.7
MoCo v2 [10]	73.9 ± 0.12	75.6 ± 0.09
BYOL [†] [23]	75.0 ± 0.22	75.8 ± 0.31
DenseCL [56]	73.8 ± 0.2	76.1 ± 0.12
DetCon _B [†] [28]	76.0 ± 0.14	76.2 ± 0.09
ReSim [60]	74.3 ± 0.28	75.5 ± 0.15
PixPro [63]	74.2 ± 0.44	75.9 ± 0.37
DetCo [61]	74.3 ± 0.07	74.9 ± 0.46
LEWEL [31]	75.5 ± 0.23	75.4 ± 0.07
<i>R2O</i>	76.7 ± 0.09	76.6 ± 0.05

Table A1: Performance on PASCAL VOC and Cityscapes semantic segmentation (mIoU) with standard deviation across 3 seeds. [†]: Results from re-implementation of pretraining method.

Method	Epochs	AP ^{bb}	AP ^{mk}
BYOL (reproduced)	300	$40.3 (\pm 0.10)$	$37.5 (\pm 0.08)$
DetCon _B (reproduced)	300	$41.5 (\pm 0.03)$	$38.0 (\pm 0.09)$
Ours	300	$41.7 (\pm 0.02)$	$38.3 (\pm 0.07)$

Table A2: Performance on COCO object detection and instance segmentation with standard deviation following the $1 \times$ schedule averaged across 3 seeds.

A.4 Exploring Contrastive Representation Learning

We investigate using a contrastive objective function for L_{repr} . We use the NT-Xent objective used by the authors of SimCLR [8] and employ the same architecture, data augmentation policy, and optimization details. We adopt the mask sampling strategy employed by Hénaff et al. [28] in order to reduce the memory overhead caused by the cross-GPU gather operation used in contrastive learning. Table A3 compares the performance when using the SimCLR objective or the BYOL objective. To ensure fair comparison, both methods were pretrained for 300 epochs on ImageNet100 using the $K = 128 \rightarrow K = 4$ schedule. The BYOL objective leads to an improvement of +4.51 on PASCAL and +1.44 on Cityscapes for the task of semantic segmentation. We note that the authors of DetCon [28] demonstrated similar results when using a contrastive objective, with DetCon_S requiring up to 3 times the pretraining in order to match the performance of DetCon_B.

Objective	PASCAL VOC	Cityscapes
SimCLR NT-Xent	62.99 \pm 0.02	69.99 \pm 0.17
BYOL	67.5 \pm 0.1	71.43 \pm 0.25

Table A3: **Comparing contrastive and Siamese representation learning objectives.** We investigate using contrastive learning, via the SimCLR NT-Xent objective, during *R2O* pretraining. We find that using a Siamese representation learning objective such as BYOL outperforms its contrastive counterpart when finetuned for PASCAL VOC (+4.51) and Cityscapes (+1.44) semantic segmentation. Results report mean mean intersection-over-union (mIOU).

A.5 Exploring Vision Transformer Architectures

Inspired by the recent progress in applications of Vision Transformer (ViT) architectures [27, 6, 11, 18], we experiment with applying *R2O* pretraining to a ViT-Base (ViT-B) architecture. We apply additional transpose convolution layers during the pretraining on the feature maps in the final transformer block to get 7x7 and 14x14 feature maps to mimic the output of ResNet C5 and C4 output. We did not make any other changes to the architecture or the loss. We pretrained the *R2O* and MAE for 300 epochs on ImageNet100 with a global batch size of 1024. We used the exact same optimization set up as our ResNet experiments. The base learning rate is 0.3 following a cosine decay schedule. The momentum is 0.9 and weight decay is 10^{-6} . For MAE, we strictly followed the optimization setting of [27]. We evaluate the pretrained weights of MS COCO for instance detection and segmentation. We finetuned for $1 \times$ schedule (12 epoch) using AdamW optimizer. The learning rate is $3e-4$, the layer-wise decay rate is 0.75, and the drop path rate is 0.2. The learning rate is multiplied by 0.1 at epochs 9 and 11. Table A4 compares MAE [27] to *R2O* when using a ViT-B encoder after pretraining on ImageNet100 for 300 epochs. The *R2O* pretrained encoder provides a +5.7 increase in AP^{bb} and a +4.9 increase in AP^{mk} relative to MAE. Thus, the benefits of *R2O* pretraining for dense prediction tasks also apply to newer architectures such as ViTs.

Objective	AP^{bb}	AP^{mk}
MAE [27]	34.8	31.7
<i>R2O</i>	40.5	36.6

Table A4: **Examining COCO object detection and instance segmentation performance when pretraining a ViT.** We report Average Precision on bounding box (AP^{bb}) and mask (AP^{mk}) predictions for val2017

A.6 Impact of Scheduler Type

We also experiment with the type of region-to-object scheduler (cosine, piecewise or linear). In our ImageNet-1K experiment, we used a cosine scheduler due to its performance in small-scale experiments. When pretraining on ImageNet100, our linear and piecewise schedule slightly outperform the cosine schedule (+0.5 and +0.3 on PASCAL VOC mIOU) (Table A5). This shows the benefit of region-to-object learning. Most importantly, *R2O* pretraining leads to better performance regardless of the type of scheduler.

A.7 Importance of Region-Level Prior

Compared with spatial heuristics, which divide an image into say a fixed number of square patches, the SLIC prior which take into account color resemblance leads to better performance (+0.8 mIOU) when finetuned for PASCAL VOC semantic segmentation (Table A5). This suggest that using a broader set of image-level criteria in equation will improve our learning process. The performance benefits of SLIC also suggest that finding good region priors is important for the refinement process. When comparing 10×10 spatial prior with 2×2 spatial prior, we see that the encoder pretrained

using the 10×10 prior performs because this prior introduces weaker spatial constraints than its 2×2 counterpart.

Prior	Scheduler	K schedule	PASCAL VOC (mIOU)
SLIC	Linear	$128 \rightarrow 4$	62.3
SLIC	Cosine	$128 \rightarrow 4$	61.8
SLIC	Piecewise	$128 \rightarrow 4$	62.1
SLIC	Fixed	128	61.4
SLIC	Fixed	64	61.4
SLIC	Fixed	4	60.7
Spatial (10×10)	Linear	$128 \rightarrow 4$	61.5
Spatial (2×2)	Linear	$128 \rightarrow 4$	60.1

Table A5: **Effect of varying region-level prior and type of region-to-object scheduler.** We pre-train on ImageNet100 for 100 epochs using various region-level priors and region-to-object schedulers (e.g. cosine, linear, or piecewise schedule). Results display the mean intersection-over-union (mIOU) after finetuning on PASCAL VOC for semantic segmentation.

A.8 Visualization of Mask Refinement

ImageNet-1K Pretraining In Figure A1, we visualize the masks generated by *R2O* in the region refinement step during pretraining. The number of segments, K , starts at 128 and gradually decreases to 4 following a cosine schedule. At 100 epoch, $K = 119$. At 200 epoch, $K = 74$. At 300 epoch, $K = 4$.

In Figure A2, we visualize some failure cases where the masks failed to capture objects. In these examples, masks group pixels that are similar in color and texture but do not belong to the same object (examples 1, 4). They also tend to over-segment an object into multiple parts if different parts have large disparities in color and texture (example 2). In a few extreme cases, the masks groups all the pixels in entire image as belonging to the same object (example 3). Since we are performing K-means over the batch, this could happen when there is large variance across region-level features in the batch while the variance in region-level features from the given image is small. However, even in this worst case scenario, our representation learning step amounts to using the standard BYOL objective with a global-pooled embedding.

COCO Pretraining We perform an additional experiment to investigate the mask refinement when pretraining on COCO, a scene-centric dataset. We use the default region-to-object scheduler used in our ImageNet-1K experiments, i.e. $K = 128 \rightarrow K = 4$, and find the quality of refined masks to be comparable to those generated during ImageNet-1K pretraining (0.46 versus 0.49 final ABO respectively). Figure A3 visualizes some of the masks by the end of COCO pretraining.

Caltech-UCSD Birds 200-2011 Segmentation We perform unsupervised segmentation on Caltech-UCSD with K-means clustering on feature space with $K=5$ using *R2O* ImageNet pre-trained checkpoints. Figure A4 visualizes some of the masks.

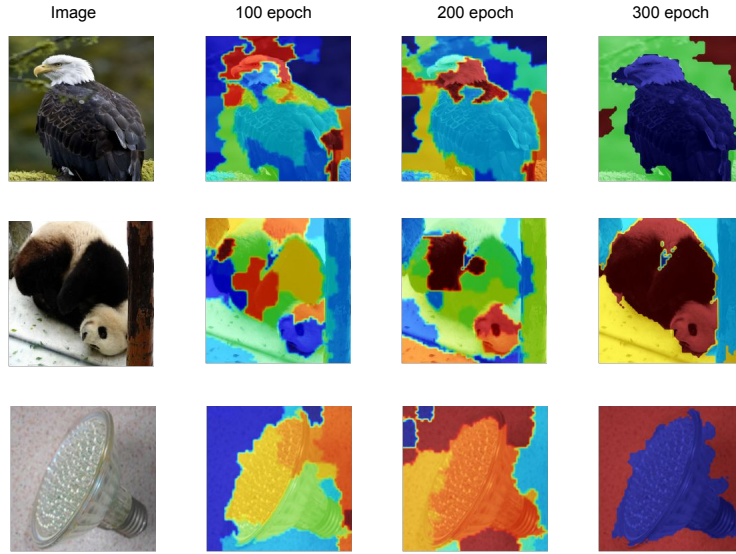


Figure A1: **Visualization of refined masks generated during ImageNet pretraining** after 100, 200 and 300 epochs. We demonstrate early masks consists of random image segments which gradually become object-centric.

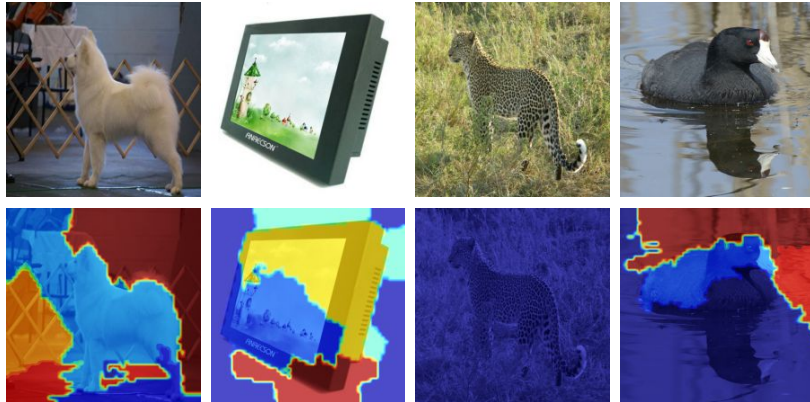


Figure A2: **Visualization of Failure Cases.** We visualize some of the poorly segmented masks generated during pretraining. From left to right: In example 1, one mask groups the dog and part of the background together because of similar colors. In example 2, the masks oversegment the TV screen into multiple regions. In example 3, the jaguar blends into the background. In example 4, the masks fail to distinguish the actual object and its reflection.



Figure A3: **Visualization of COCO Pretraining.** We pretrain the model on COCO and visualize the K-means mask during the training. The columns from left to right are original images, SLIC regions priors and clustering results.

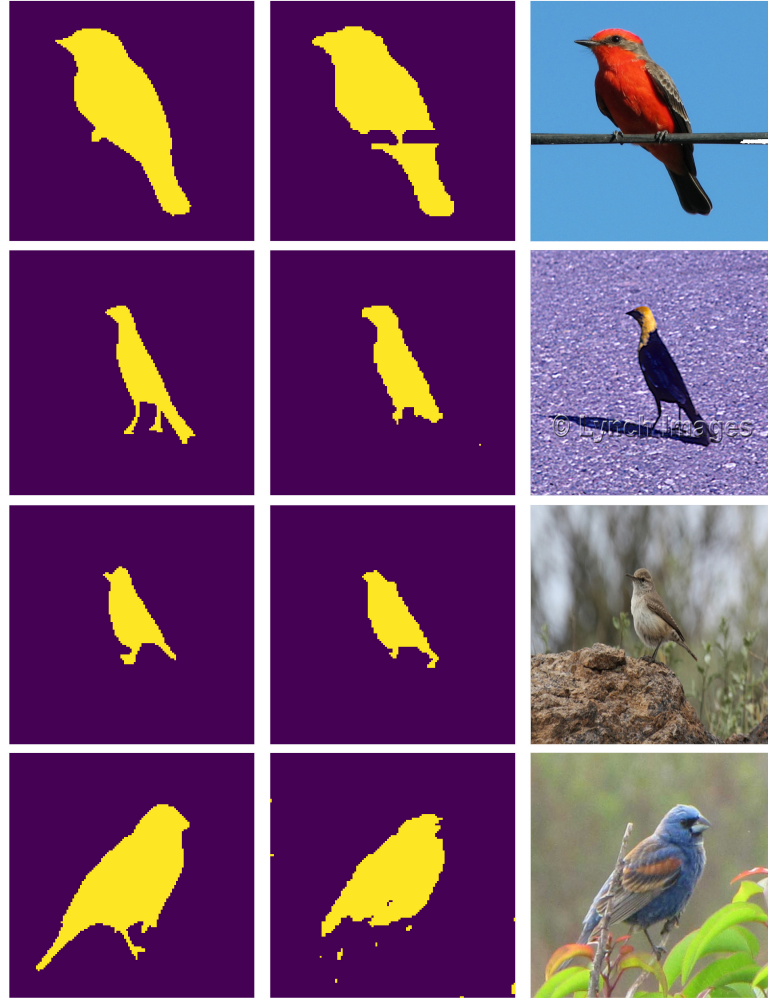


Figure A4: **Visualization of Caltech-UCSD Birds 200-2011 Segmentation.** We perform unsupervised segmentation by clustering feature representations on a per-image basis with $K = 5$. The best match is considered as the foreground.